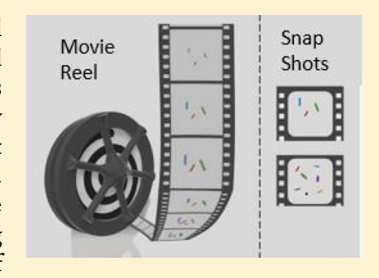
Cite This: Mol. Pharmaceutics 2020, 17, 769-776

# In Situ Crystal Growth Rate Distributions of Active Pharmaceutical **Ingredients**

Sreya Sarkar,<sup>†,§</sup> Zhengtian Song,<sup>†,§</sup> Scott R. Griffin,<sup>†</sup> Nita Takanti,<sup>†</sup> Andrew D. Vogt,<sup>‡</sup> Alexander Ruggles,<sup>‡</sup> Gerald D. Danzer,<sup>‡</sup> and Garth J. Simpson\*,<sup>†</sup>

Supporting Information

**ABSTRACT:** Single-particle tracking of crystal growth performed in situ enables substantial improvements in the signal-to-noise ratio (SNR) for recovered crystal nucleation and growth rates by nonlinear optical microscopy. Second harmonic generation (SHG) is exquisitely sensitive to noncentrosymmetric crystals, including those produced by many homochiral active pharmaceutical ingredients (APIs). Accelerated stability testing at elevated temperatures and relative humidity informs design of pharmaceutical formulations. In the present work, we demonstrate reduction in the Poisson noise associated with the finite number of particles present in a given field of view through continuous monitoring during stability testing. Single-particle tracking enables recovery of crystal growth rates of individual crystallites and enables unambiguous direct detection of nucleation events.



Collectively, these capabilities provide significant improvements in the signal-to-noise for nucleation and crystal growth measurements, corresponding to approximately an order of magnitude reduction in anticipated measurement time for recovery of kinetics parameters.

KEYWORDS: amorphous solid dispersions, second harmonic generation, microscopy, single particle tracking, crystal growth kinetics

#### INTRODUCTION

Downloaded via PURDUE UNIV on January 7, 2021 at 15:17:26 (UTC). See https://pubs.acs.org/sharingguidelines for options on how to legitimately share published articles.

Production of amorphous solid dispersions (ASDs) offers a broadly applicable approach for kinetically circumventing solubility limitations of poorly soluble active pharmaceutical ingredients (APIs). In an ASD, the API is cast in a glassy polymer matrix with relatively high aqueous solubility, such that the API is forced into solution upon dissolution of the matrix.<sup>1–4</sup> When optimizing a polymer/excipient/API cocktail for preparing final dosage forms, one critical consideration is the long-term stability of the API within the ASD. Concentrating the API in the ASD to minimize the total mass load of the final dosage form is balanced by a desire to also reduce the chances of API nucleation and crystallization during storage of the ASD. For poorly soluble APIs, the crystalline form often exhibits negligible bioavailability, passing through the digestive tract for oral final dosage forms. In intravital formulations, residual insoluble API particulates can pose additional risks from inducing foreign body embolism. 5-8 For these reasons, stability testing is widely used to inform the optimization of final dosage forms. High-throughput testing requires a host of different test materials, multiple replicates of which at multiple time points are required for stability assessment over long timeframes (up to year-long timeframes). The high throughput, high sampling rate, and long incubation times (weeks to months) can significantly complicate sample preparation and storage capacities even when using accelerated conditions.

The duration of stability testing is ultimately dictated by the sensitivity with which crystal formation can be quantified for informing kinetic modeling, with a suite of methods currently brought to bear to address this measurement challenge. These include polarized light microscopy (PLM),9,10 X-ray powder diffraction (PXRD), 11,12 differential scanning calorimetry (DSC), 10,13,14 Raman spectroscopy, 15,16 Fourier transform infrared spectroscopy (FTIR), 15,17,18 and solid state nuclear magnetic resonance (sNMR). 15,19 PLM is one of the most common methods used for determining the presence of crystalline content in stability testing. Despite its widespread use, PLM can only provide qualitative information on optically transparent samples and is commonly complicated by interference from occlusions, contaminants, and crystalline excipients. As a consequence, PLM is challenging to integrate into fully automated quantitative analyses of crystallinity. PXRD is arguably the current "gold standard" for detecting trace crystallinity within the pharmaceutical industry but generally does not enable quantification at low crystallinity, takes several minutes for sample preparation/analysis, and requires several mg of material for analysis. A large dynamic range with correspondingly low limits of detection has multiple benefits in accelerated stability testing, including (i) improved

September 9, 2019 Received: Revised: November 15, 2019 Accepted: November 26, 2019

Published: November 26, 2019



Department of Chemistry, Purdue University, 560 Oval Drive, West Lafayette, Indiana 47907, United States

<sup>\*</sup>AbbVie Inc., 1 N Waukegan Road, North Chicago, Illinois 60064, United States

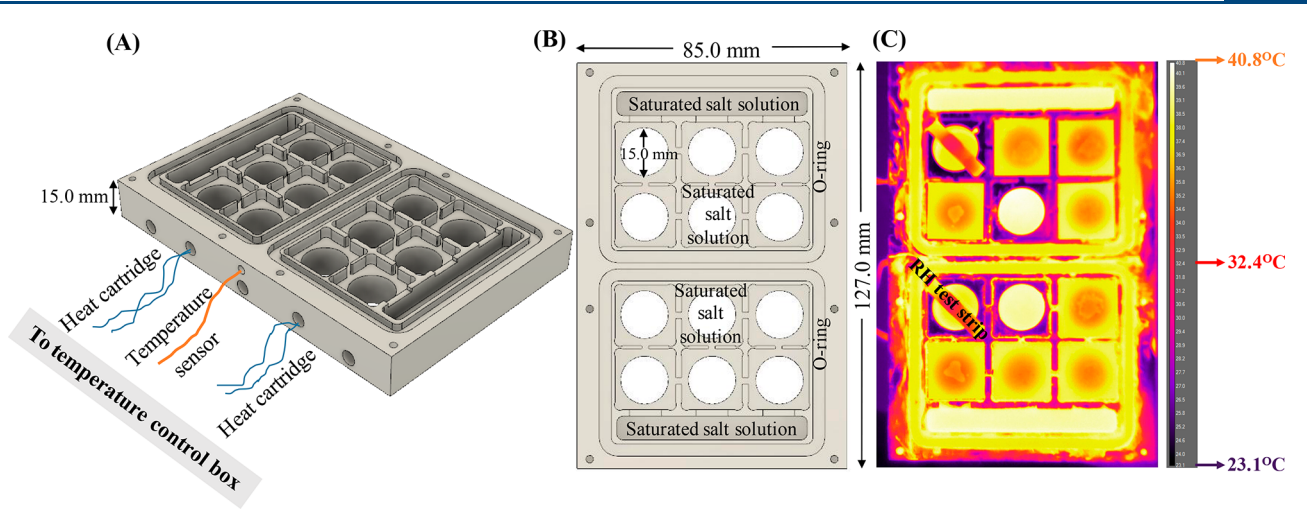


Figure 1. (A,B) CEiST design, (C) IR thermal image of CEiST for validation of set temperature at 40 °C.

statistical confidence in kinetics parameters, (ii) simplified kinetic modeling without the need to account for depletion effects, (iii) compatibility with low-API-load ASDs, (iv) reduced volumes for sample storage during testing, and (v) reduction in the timeframe necessary for decision-making in stability assessments. For the majority of the methods routinely used for API analysis, limits of detection are on the order of a fraction of a percent, providing a relatively narrow dynamic range in crystalline API detection; in some cases, the total drug loading may only be on the order of a few percent.

In addition to the limited dynamic range, the majority of these common analysis tools probe only ensemble-average behaviors, masking possible intrinsic heterogeneity in crystal nucleation and growth kinetics. For example, it is well-established that the nucleation and growth kinetics can differ substantially for crystals generated on the surfaces of ASD particles and glassy APIs relative to the bulk. 18,20 Even in homogeneous media, subtle differences in local environment can produce variance in crystal growth rates. 1 The impact of this variance in growth kinetics on subsequent performance remains unresolved, due in part to the dearth of methods currently available to quantitatively inform the inherent variation in single-particle growth kinetics.

Nonlinear optical imaging has the potential to provide the limits of detection required for investigating single-particle growth kinetics and fill this knowledge gap. Nonlinear optics has recently gained traction in the pharmaceutical industry for sensitive detection and quantification of trace crystalline content within amorphous formulations. 11,22-26 Second harmonic generation (SHG) describes the coherent conversion of light to twice the frequency, which is symmetry-forbidden in centrosymmetric media but allowed in assemblies of lower symmetry, including the large majority of noncentrosymmetric crystals. SHG provides a near background free measurement of the crystalline fraction of an ASD, since the disordered, amorphous material will not produce coherent SHG. Due to the sensitivity and selectivity of SHG, routine measurements can be made with a limit of detection in the ppm regime.<sup>2</sup> Utilizing the sensitivity of SHG to crystalline content for identification of regions of interest, the detection limits for Raman<sup>5,28</sup> and XRD<sup>29</sup> have been lowered into the ppm regime as well. The low limits of detection of SHG microscopy enabled quantification of crystallization kinetics in ASDs spanning a 4 order of magnitude range in crystallinity. 27,30

In this work, the quantitative capabilities of SHG analysis are substantially improved further, while the total sample volume and storage burden are dramatically reduced through in situ analysis. A controlled environment for in situ stability testing (CEiST) was developed to leverage the sensitive, non-destructive analysis capabilities of SHG for continuous monitoring of individual crystallites during nucleogenesis and growth. The CEiST platform allowed for single-particle tracking over hours to days under accelerated stability conditions typical for ASD analysis. Monitoring the same fields of view over time lowered noise in determinations of the nucleation rates and crystal growth rates obtained from accelerated stability tests while simultaneously lowering the amount of sample required.

## **EXPERIMENTAL METHODS**

ASD samples of ritonavir (15%), sorbitan monolaurate (10%), copovidone (74%), and colloidal silicon dioxide (1%) were prepared at AbbVie as spray dried dispersions (SDDs) and hot melt extrudates (HMEs). Samples without the sorbitan monolaurate were also made, in which the copovidone weight percent was increased to 84%. HME samples were milled prior to use. The extrudates were made using a lab scale Thermo Scientific Process 11 Hygienic Parallel twin-screw extruder fed gravimetrically at 0.750 kg/h with a screw speed of 250 rpm. Temperatures in the heating zones ranged from 15 to 150 °C. The extrudates were milled using a Fitzmill L1A at 6000 rpm and a screen size of 0.033 in round hole. The ASDs by SDD were made using a Büchi B-290 spray dryer with an inert loop using methanol as the solvent. The feed solution flow rate into the two-fluid nozzle (1.4 mm diameter) was 20 g/min, with nitrogen atomizing gas. The nitrogen process gas was set to 30 kg/h. The inlet and outlet temperatures were 90 and ~50 °C, respectively, while the condenser was held at -20 °C. All powder samples were placed into the CEiST chamber or into a standard stability chamber as thin layers ( $\sim 300 \ \mu m$ ).

The CEiST's design is shown in Figure 1. The CEiST consists of an aluminum block machined to house two sections separated by greased O-rings. Each compartment was kept at different RHs depending on the saturated salt solution put into the two reservoirs within each compartment and by sealing each compartment with a plexiglass window and aluminum sleeve held in place by screws. The aluminum sleeve was machined to allow imaging through each well in the main body

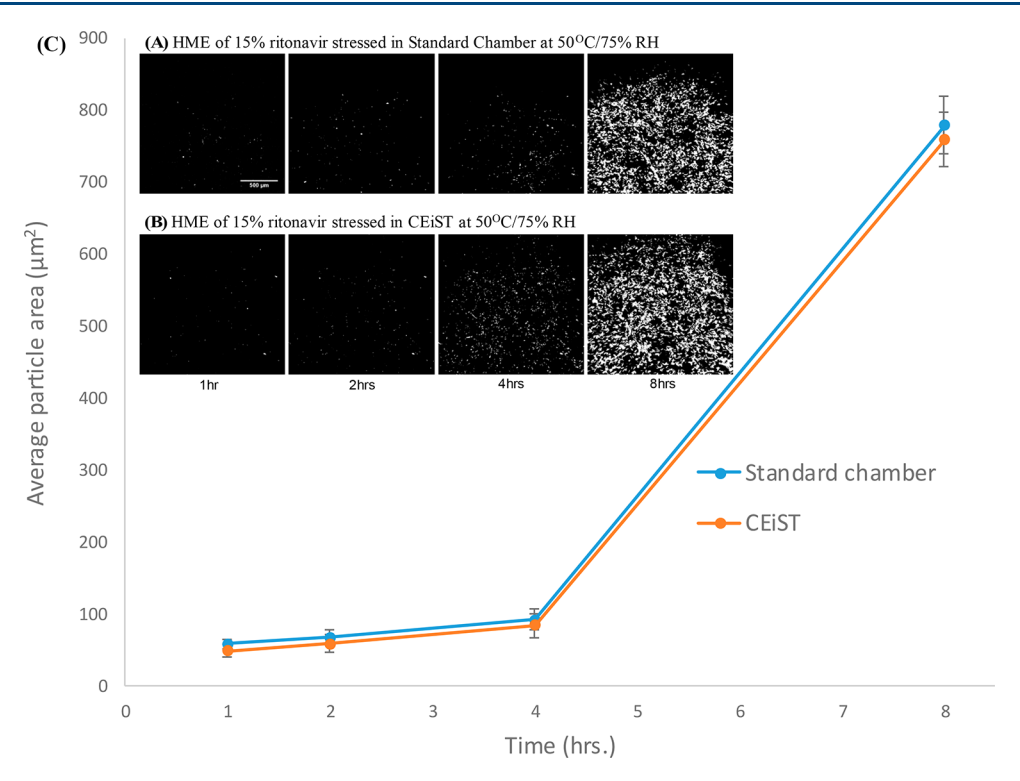


Figure 2. SHG images for time-dependent crystal growth of 15% HME ritonavir in (A) standard chamber and in (B) CEiST. (C) The plot for average particle areas shows good agreement between the two different methods.

of the CEiST, while heat was provided to the outside of the plexiglass to prevent condensation. Both compartments of the device were kept at an elevated RH of 75% through all experiments by using a saturated NaCl solution. The RH in each compartment of the CEiST was validated using reversible Moisture Indicator strips (Indigo Instruments, 33813-2080). Once each compartment was validated, the indicator strips were no longer used during experiments. The temperature was controlled by using two Tempco low-density cartridge heaters (LDC00003) placed at different locations on the CEiST and a thermocouple in the center for feedback control by a custom controller built by the Johnathan Amy Facility for Chemical Instrumentation at Purdue, depicted in Figure 1(A). An IR thermal image of the CEiST in Figure 1(C) confirmed uniform temperature within ±2 °C of the set point temperature. Samples were placed onto coverslips and then onto one of the 10 wells within the CEiST. For comparative purpose, a standard stability chamber was made by placing saturated sodium chloride solution into the bottom of a desiccator wrapped in heat tape. The temperature of the entire chamber was monitored by thermocouple feedback.

Accelerated stability tests were performed using a SONICC microscope from Formulatrix (Bedford MA) for SHG imaging that was modified in house for epi detection. For the in situ stability testing, samples in the CEiST chamber were maintained at an elevated temperature and humidity during SHG imaging. For samples maintained in the standard stability chamber, aliquots were sampled at select time points, analyzed by SHG under ambient conditions, and then discarded. The time from stability chamber removal through testing was about 10 min. Experiments were performed using ~200 mW excitation laser power at the sample and 890 ms exposure time, repeated every hour (duty cycle of  $2.8 \times 10^{-4}$ ). SHG was measured in the transmission direction due to the high

transparency of samples in the CEiST through hygroscopic water uptake by the ASD. SHG was collected in the epi direction for powdered samples before being subjected to elevated temperature and humidity. For samples within the standard chamber, three fields of view were used for each time point. For samples within the CEiST, several fields of view were selected from each of the three wells prepared for each ASD.

## ■ RESULTS AND DISCUSSION

The performance of the CEiST was evaluated relative to a conventional temperature and humidity controlled chamber through side-by-side comparisons of accelerated stability testing of 15% DL (w/w) ritonavir ASDs with HME at 50 °C/75%RH, the results of which are summarized in Figure 2. The amorphous excipients present in the HME ASDs did not produce significant coherent SHG signal. In contrast, ritonavir crystals adopted an SHG-active noncentrosymmetric lattice upon crystallization, enabling selective detection of crystalline ritonavir in HME ASDs using a particle counting algorithm.<sup>31</sup> SHG images at four representative time points are shown in Figure 2(A) for ASDs stored in a standard chamber at elevated temperature and humidity and in Figure 2(B) for ASDs stored in the CEiST under identical target conditions. For quantitative comparison of ritonavir crystallization between the two platforms, the average crystal area at each time point was recovered by particle counting, shown in Figure 2(C). The error bars in Figure 2(C) represent the standard deviations of three fields of view for each time point. The SHG micrographs and the average crystal areas observed for both the standard chamber and the CEiST platform were in excellent agreement, suggesting that the conditions produced in the CEiST platform are representative of those experienced in conventional temperature and humidity controlled chambers.

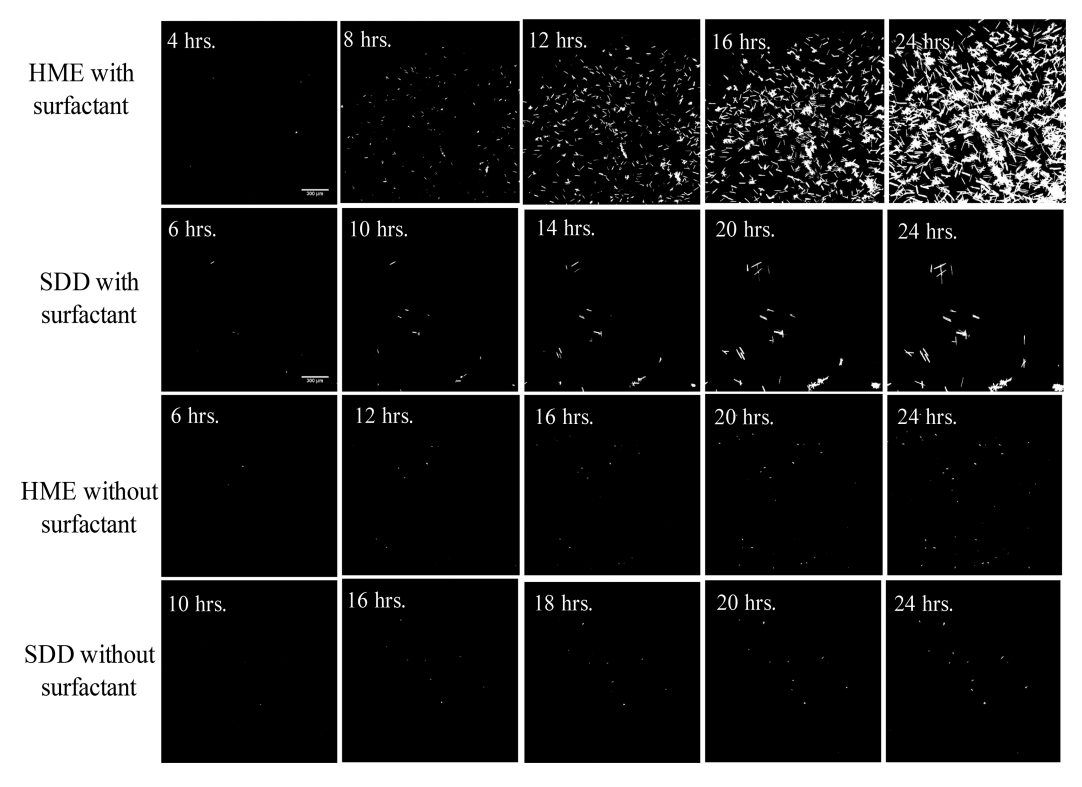


Figure 3. Time-dependent SHG micrographs of 15% ritonavir ASDs in the CEiST at 50  $^{\circ}$ C/75%RH.

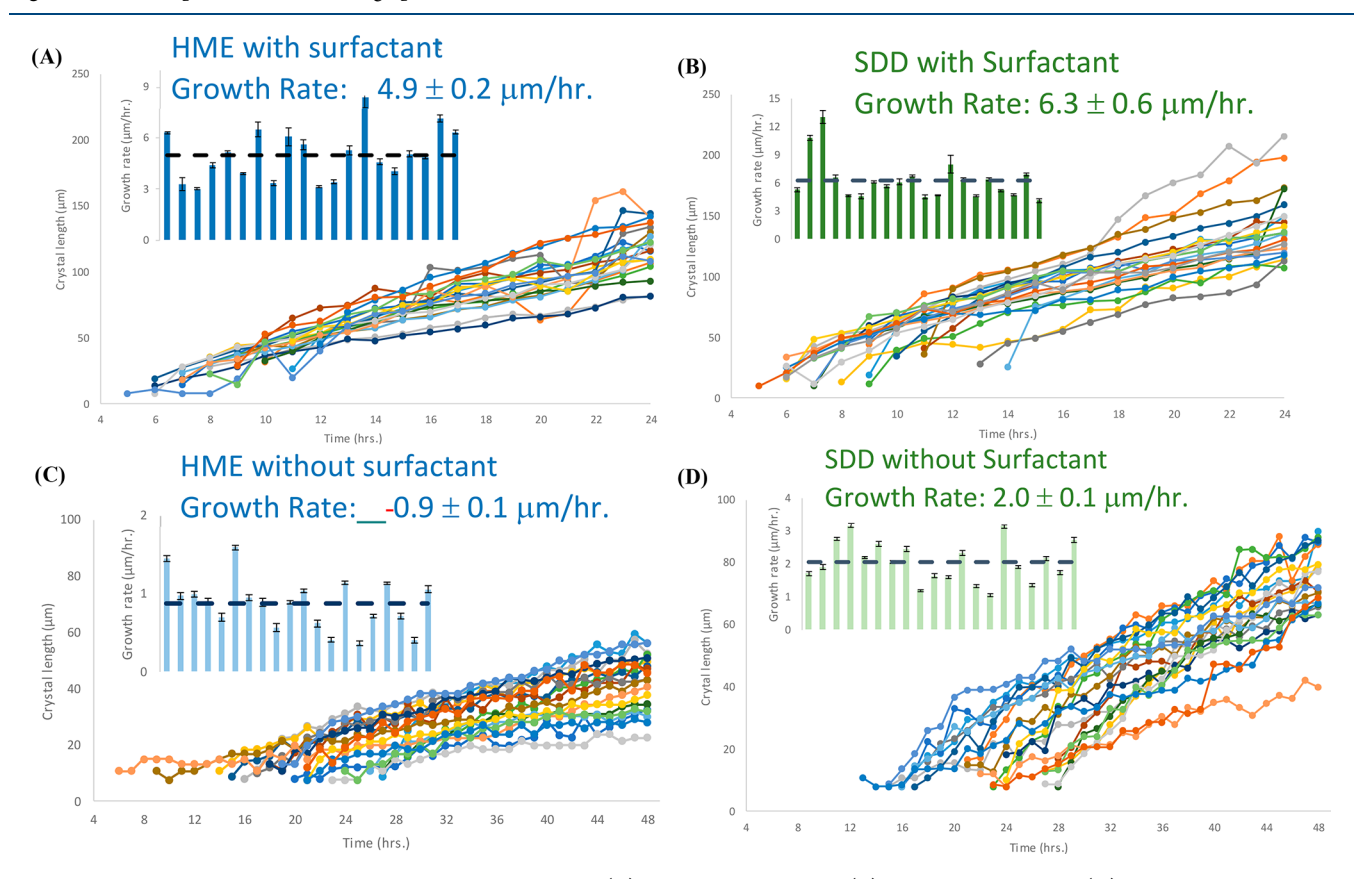


Figure 4. Individual crystal growth distribution in the CEiST for (A) HME with surfactant, (B) SDD with surfactant, (C) HME without surfactant, and (D) SDD without surfactant. Each plot has 20 different crystals tracked along the entire time trace and selected from different FOVs. The inset in each plot shows the dispersion in growth rates with the average growth rates shown in each plot as a dashed line.

Using the CEiST platform, 10 trials of in situ accelerated stability testing were run in parallel for ritonavir crystallization

in different ASDs at 50 °C and 75% RH. The ASDs were prepared with different components and different manufactur-

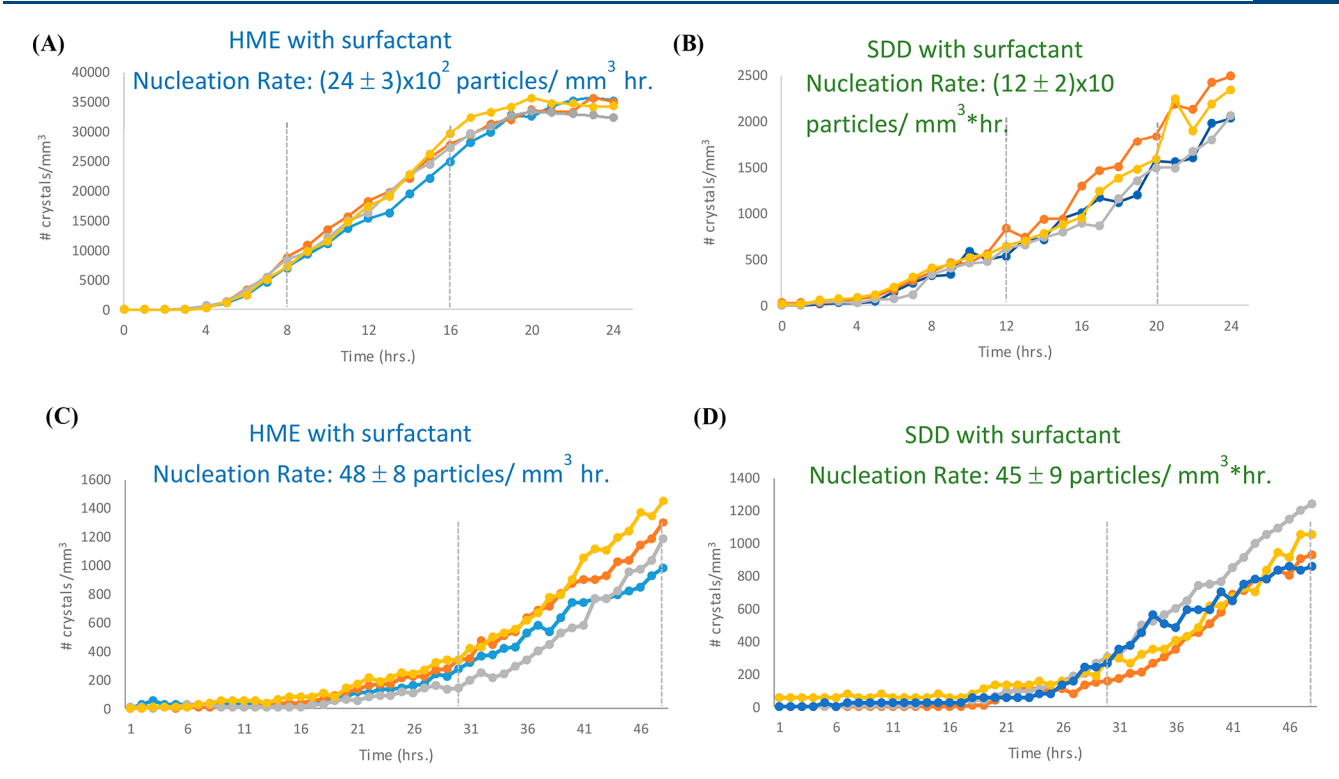


Figure 5. Average nucleation rates and single-FoV trajectories in the CEiST for (A) HME with surfactant, (B) SDD with surfactant, (C) HME without surfactant, and (D) SDD without surfactant.

ing techniques (see Experimental Methods). The ASD powder samples were examined by SHG microscopy and initially showed no detectable epi-SHG signal (i.e., no continuous regions of interest with at least three contiguous pixels of at least three counts). From previous studies using SHG to interrogate ASDs, this criterion corresponds to a lower limit of detection of 10 ppm crystallinity, 30 indicating that the initial crystallinity in all cases was less than this lower limit of detection.

The SHG images and corresponding bright field images were automatically collected every hour starting from 0 to 48 h. Four sets of representative SHG images at five different time points are shown in Figure 3. All of the images are shown with the same brightness scale for comparison. Based on the time-dependent SHG images, the incorporation of surfactant (Span 20) increased the ritonavir nucleation rate and crystal growth rate in ASDs. In this case, the addition of Span 20 resulted in more crystals and larger crystal size in accelerated stability testing, consistent with the presence of Span 20 significantly reducing the stability of ritonavir against crystal formation in both hot melt extruded and spray dried ASDs. Compared with SDD ASDs, HME samples showed a greater number of crystals and lower induction times in the accelerated stability testing. Images for later time points (25–48 h) are shown in Figure S1.

When accelerated stability testing was performed by using the standard temperature and humidity control chamber, the sample aliquots were taken out of the controlled environment to enable SHG imaging under ambient conditions. Since temperature and humidity cycling can significantly change the crystallization kinetics (Figure S2), all the samples using the standard chamber were discarded following SHG imaging. The perturbations associated with temperature cycling are attributed to a two-step process: (i) increase in supersaturation upon cooling to room temperature, resulting in increased

nucleation rate, followed by (ii) increased diffusion upon return to elevated temperature and humidity, resulting in increased crystal growth rates. Multiple aliquots of sample were therefore required to collect images at different time points using conventional stability chambers to avoid kinetic artifacts from temperature cycling. This practice was in stark contrast to measurements performed using the CEiST system, which supported continuous monitoring of the same fields of view within a sample under controlled conditions.

For each sample in the CEiST system, single-particle tracking was performed to monitor the growth rates of individual particles, representative results of which are shown in Figure 4(A–D), selected from four to six different fields of view. The long axes of the needle-like ritonavir crystals (Form II) were used to quantify crystal size. The dispersion in crystal growth rates is shown in the inset plots of Figure 4. For individual crystals, error bars in the growth rates were assessed from the standard error of the slope of crystal size versus time. From inspection of the histograms of single-crystal growth rates and the standard errors, it is clear that the dispersion in growth rates exceeds experimental uncertainties and therefore reflects an intrinsic diversity in single-crystal growth kinetics within the samples.

Single-particle tracking enabled by the CEiST platform provided substantial signal-to-noise benefits in nucleation kinetics as well. The average nucleation rates were found from the linear growth regime shown in Figure 5(A-D) by linear fitting of nucleation events from four different fields of view. The uncertainties reported in each plot arise from the variabilities of the fields of view. The linear region for fitting was marked by the dashed line. The nucleation rate in HME ASDs in Figure 5(A) is 1 order of magnitude higher than in the SDD shown in Figure 5(B), in the presence of 10% Span 20 in the ASDs. The residual nuclei present in HME ASDs might be

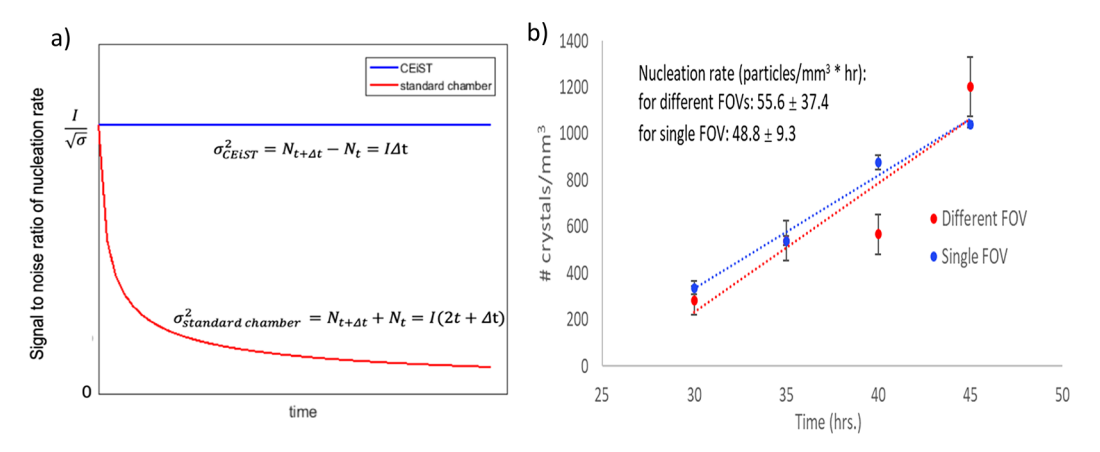


Figure 6. (a) The anticipated signal-to-noise ratio of the nucleation rate for in situ vs conventional stability testing based on the Poisson statistics of crystal counting. I = nucleation rate,  $\sigma$  = uncertainty of nucleation rate based on Poisson statistics,  $N_t$  = number of crystals at time t. (b) A comparison between the results from a standard chamber and the CEiST. The different FOV represents the standard chamber where four time points were taken from four different repititions of the same experiment, and the single FOV is from a single experiment in the CEiST.

responsible for producing this higher nucleation rate. However, without the presence of Span 20, the ritonavir nucleation rates are similar in both HME and SDD at the RH and temperatures evaluated.

The substantial improvement in signal-to-noise for nucleation rate determination in the CEiST can be understood considering the Poisson statistics associated with crystal genesis in combination with the sensitivity of SHG imaging to support single-particle tracking. Nucleation rates using a standard stability chamber were calculated from the differences in the number of crystals between multiple independent samples analyzed at different time points. Because each sample is statistically independent, the number of crystals in any given field of view (FOV) is given by a Poisson distribution. As a result, the nucleation rate is generated from the difference between two Poisson-distributed numbers acquired at different time points. In the linear kinetics regime, the number of previously nucleated crystals contributes to the uncertainty in the number of new particles, rapidly degrading the precision to which the number of new particles can be determined based on Poisson statistics. In contrast, the nucleation rates in the CEiST chamber were calculated from the differences in the numbers of new crystals within the same single FoV, removing all statistical uncertainties regarding the number of pre-existing crystals. As such, uncertainty in the nucleation rate is defined only by the Poisson statistics for the number of new particles within a given FoV. The signal-to-noise advantage associated with nucleation rates determined from analysis of single samples versus stochastic sampling is shown in Figure 6. Following the initial onset of nucleation, Poisson-distributed uncertainties in the differences in particle numbers between independent samples rapidly degrade the precision to which nucleation rates can be determined. However, no such statistical loss in SNR is expected from repeated analysis of a single FoV.

Interestingly, the SNR improvement afforded by single-particle tracking pairing SHG microscopy with the CEiST platform provides a simultaneous advantage in reducing sample volume requirements. Stability testing of pharmaceutical formulations can extend over several weeks, months, or even years, for each of potentially many different formulation candidates. The temperature cycling complication coupled with the Poisson statistics limitations of standard crystal

analysis pose cost challenges associated with archiving large volumes of identical replicate samples in controlled environments for testing times spanning multiple months or years. Continuous in situ monitoring of a single field of view over the entire time course of a stability assessment (e.g., by SHG microscopy) provides reduction in sample volume requirements proportional to the number of time points used for kinetics assessments. For example, in the present study with up to 48 time points recorded for a given sample, the total assay volume is correspondingly reduced up to 48-fold.

The collective results of the single-particle tracking experiments provide insights into the molecular connections between stability, method of preparation, and composition of ASDs. The higher observed crystal growth rate in SDD relative to HME ASDs suggests a fundamental difference in the molecular diffusion coefficient within the matrices, as the ritonavir growth rate is diffusion limited in this regime. The origin of this disparity in diffusion coefficients may potentially be attributed to the desolvation step in SDD generation, which may potentially produce a higher density of microscopic voids in the final products and higher molecular diffusion. Presence of Span 20 in ASD formulations of ritonavir contributes to processability but dramatically increases molecular diffusion, with corresponding increases in single-crystal growth rates. Specifically, the surfactant Span 20 increased the crystal growth rate by  $\sim$ 5 times for the HME and  $\sim$ 3 times for the SDD.

The surfactant, Span 20, induced ~50-fold and ~20-fold changes in nucleation rates for HME (2400  $\pm$  300 to 48  $\pm$  8 particles/mm<sup>3</sup>·hr) and SDD (120  $\pm$  20 to 45  $\pm$  9 particles/ mm<sup>3</sup>·hr), respectively. The nucleation kinetics are also distinctly different between SDD and HME ASDs in the presence of Span 20, with nucleation rates about an order of magnitude higher in HME. This difference in nucleation rate may potentially arise from the presence of residual nuclei within the melt in the HME materials from incomplete melting.<sup>34</sup> Optimization of conditions for HME preparation strikes a balance between the competing desires for higher temperatures to remove residual nuclei and lower temperatures to minimize pyrolysis. As such, the presence of trace residual nuclei within the HME is arguably more likely than in the SDD materials, consistent with the observations made by singleparticle tracking by SHG microscopy.

Recovery of the crystal growth rate distribution from singleparticle tracking suggests the presence of subtle but significant heterogeneity within the samples at microscopic scales. From inspection of the individual single-particle growth curves in Figures 4, it is clear that the particle-to-particle differences in growth rates exceed experimental uncertainties of the fits, indicating that the differences are statistically significant. Several mechanisms were considered for potentially explaining the observed variance in crystal growth rates. Ritonavir is wellknown to adopt multiple crystal polymorphs, each of which would presumably adopt unique growth kinetics. However, previous studies of similarly prepared ritonavir samples confirmed by IR and XRD the exclusive presence of Form II.<sup>30</sup> Furthermore, the ritonavir crystals all exhibited similar aspect ratios and crystal habits, consistent with expectations for the presence of a single-crystal form. As an alternative explanation for the variance in single-particle growth kinetics, the influence of crystal orientation was considered. Experiments were performed in which crystals serving as seeds were placed on the surface of a 15% ritonavir HME film, such that the rod-like crystals were similarly oriented with the long axis within the surface plane. Despite the monodispersity in orientation, individual crystals still produced statistically distinct growth rates, suggesting that orientation was not a primary factor for the variance in single-particle growth kinetics (Figure S3). This intrinsic variability in growth rates for nominally identical crystal forms suggests heterogeneity in local diffusivity within the surrounding matrix. The growth rate dispersion might result from subtle variation in local density, hydrophobicity, chemical composition, and so on. The diversity in growth rates and correspondingly diversity in local environments is similar between different formulations.

## CONCLUSION

The CEiST platform developed in this work enabled single-particle tracking during accelerated stability testing of ritonavir ASDs by SHG microscopy. The high selectivity of SHG to crystalline content provides high-contrast images over a large dynamic range of crystallinity for kinetics analysis. The advantage of monitoring the same field of view over time facilitated substantial signal-to-noise improvements for nucleation and growth rate assessments, supported single-particle tracking, and reduced the sample volume requirements by  $\sim\!50$  fold. From the single-particle tracking measurements by SHG microscopy, the heterogeneity in crystal growth rates within the ASDs suggests subtle but non-negligible local diversity in physical and/or chemical characteristics of the sample.

## ASSOCIATED CONTENT

## **S** Supporting Information

The Supporting Information is available free of charge at https://pubs.acs.org/doi/10.1021/acs.molpharmaceut.9b00937.

Figure S1: SHG micrographs for later time traces for HME and SDD without surfactant. Figure S2: Temperature/RH cycling effect on ASD crystallization kinetics. Figure S3: Crystal growth rates from seeded crystals all aligned on the same plane. (PDF)

## AUTHOR INFORMATION

## **Corresponding Author**

\*E-mail: gsimpson@purdue.edu.

#### ORCID ®

Sreya Sarkar: 0000-0002-1614-3730 Garth J. Simpson: 0000-0002-3932-848X

#### **Author Contributions**

§S.S. and Z.S. contributed equally to this work

#### **Notes**

The authors declare the following competing financial interest(s): A.D.V. and G.D.D. are employees of AbbVie and may own AbbVie stock. AbbVie helped sponsor and fund the study, contributed to the design, and participated in the collection, analysis, and interpretation of data and in writing, reviewing, and approval of the final publication. The other authors declare no conflicts of interest related to this work.

## ACKNOWLEDGMENTS

The authors gratefully acknowledge funding for the present work from the National Science Foundation through an NSF-GOALI award-1710475 and the U.S. Department of Education through the pharmaceutical engineering 2015 GAANN award-P200A150136. In addition, S.S., Z.S., S.R.G., and G.J.S. acknowledge financial support from AbbVie. S.S. also acknowledges support from an NSF research supplement award-1643745. The authors would also like to acknowledge Formulatrix for the use of SONICC instrumentation and Dr. Hartmut Hedderich, Randy Replogle, and Casey J. Smith for their assistance in design and construction of the CEiST platform.

## REFERENCES

- (1) Kennedy, M.; Hu, J.; Gao, P.; Li, L.; Ali-Reynolds, A.; Chal, B.; Gupta, V.; Ma, C.; Mahajan, N.; Akrami, A.; Surapaneni, S. Enhanced Bioavailability of a Poorly Soluble VR1 Antagonist Using an Amorphous Solid Dispersion Approach: A Case Study. *Mol. Pharmaceutics* **2008**, *5* (6), 981–993.
- (2) Lakshman, J. P.; Cao, Y.; Kowalski, J.; Serajuddin, A. T. M. Application of Melt Extrusion in the Development of a Physically and Chemically Stable High-Energy Amorphous Solid Dispersion of a Poorly Water-Soluble Drug. *Mol. Pharmaceutics* **2008**, 5 (6), 994–1002
- (3) Serajuddin, A. T. M. Solid dispersion of poorly water-soluble drugs: Early promises, subsequent problems, and recent breakthroughs. *J. Pharm. Sci.* **1999**, *88* (10), 1058–1066.
- (4) Williams, R. O.; Watts, A. B.; Miller, D. A. Preface. Formulating Poorly Water Soluble Drugs, 2nd ed.; Springer, 2016; Vol. 22, pp VII—IX
- (5) Schmitt, P. D.; Trasi, N. S.; Taylor, L. S.; Simpson, G. J. Finding the Needle in the Haystack: Characterization of Trace Crystallinity in a Commercial Formulation of Paclitaxel Protein-Bound Particles by Raman Spectroscopy Enabled by Second Harmonic Generation Microscopy. *Mol. Pharmaceutics* **2015**, *12* (7), 2378–2383.
- (6) Fang, C.; Bhattarai, N.; Sun, C.; Zhang, M. Q. Functionalized Nanoparticles with Long-Term Stability in Biological Media. *Small* **2009**, *5* (14), 1637–1641.
- (7) Neuberger, T.; Schopf, B.; Hofmann, H.; Hofmann, M.; von Rechenberg, B. Superparamagnetic nanoparticles for biomedical applications: Possibilities and limitations of a new drug delivery system. *J. Magn. Magn. Mater.* **2005**, 293 (1), 483–496.
- (8) Wang, S. H.; Xu, T.; Yang, Y. H.; Shao, Z. Z. Colloidal Stability of Silk Fibroin Nanoparticles Coated with Cationic Polymer for Effective Drug Delivery. ACS Appl. Mater. Interfaces 2015, 7 (38), 21254–21262.
- (9) Carlton, R. A. Polarized Light Microscopy. *Pharmaceutical Microscopy* **2011**, 7–64.

(10) Gupta, P.; Kakumanu, V. K.; Bansal, A. K. Stability and solubility of celecoxib-PVP amorphous dispersions: A molecular perspective. *Pharm. Res.* **2004**, *21* (10), 1762–1769.

- (11) Ghebremeskel, A. N.; Vemavarapu, C.; Lodaya, M. Use of surfactants as plasticizers in preparing solid dispersions of poorly soluble API: Stability testing of selected solid dispersions. *Pharm. Res.* **2006**, 23 (8), 1928–1936.
- (12) Newman, A. W.; Byrn, S. R. Solid-state analysis of the active pharmaceutical ingredient in drug products. *Drug Discovery Today* **2003**, *8* (19), 898–905.
- (13) Baird, J. A.; Taylor, L. S. Evaluation of amorphous solid dispersion properties using thermal analysis techniques. *Adv. Drug Delivery Rev.* **2012**, *64* (5), 396–421.
- (14) Yoshihashi, Y.; Iijima, H.; Yonemochi, E.; Terada, K. Estimation of physical stability of amorphous solid dispersion using differential scanning calorimetry. *J. Therm. Anal. Calorim.* **2006**, 85 (3), 689–692.
- (15) Bugay, D. E. Characterization of the solid-state: spectroscopic techniques. *Adv. Drug Delivery Rev.* **2001**, 48 (1), 43–65.
- (16) Taylor, L. S.; Zografi, G. The quantitative analysis of crystallinity using FT-Raman spectroscopy. *Pharm. Res.* **1998**, *15* (5), 755–761.
- (17) Ng, Y. C.; Yang, Z. Y.; McAuley, W. J.; Qi, S. Stabilisation of amorphous drugs under high humidity using pharmaceutical thin films. *Eur. J. Pharm. Biopharm.* **2013**, 84 (3), 555–565.
- (18) Yang, Z. Y.; Nollenberger, K.; Albers, J.; Moffat, J.; Craig, D.; Qi, S. The effect of processing on the surface physical stability of amorphous solid dispersions. *Eur. J. Pharm. Biopharm.* **2014**, *88* (3), 897–908.
- (19) Harris, R. K. NMR studies of organic polymorphs & solvates. *Analyst* **2006**, *131* (3), 351–373.
- (20) Sun, Y.; Zhu, L.; Wu, T.; Cai, T.; Gunn, E. M.; Yu, L. Stability of Amorphous Pharmaceutical Solids: Crystal Growth Mechanisms and Effect of Polymer Additives. *AAPS J.* **2012**, *14* (3), 380–388.
- (21) Li, L.; Fijneman, A. J.; Kaandorp, J. A.; Aizenberg, J.; Noorduin, W. L. Directed nucleation and growth by balancing local supersaturation and substrate/nucleus lattice mismatch. *Proc. Natl. Acad. Sci. U. S. A.* **2018**, *115* (14), 3575–3580.
- (22) Chowdhury, A. U.; Zhang, S. J.; Simpson, G. J. Powders Analysis by Second Harmonic Generation Microscopy. *Anal. Chem.* **2016**, 88 (7), 3853–3863.
- (23) Kissick, D. J.; Wanapun, D.; Simpson, G. J. Second-Order Nonlinear Optical Imaging of Chiral Crystals. *Annu. Rev. Anal. Chem.* **2011**, *4*, 419–437.
- (24) Schmitt, P. D.; DeWalt, E. L.; Dow, X. Y.; Simpson, G. J. Rapid Discrimination of Polymorphic Crystal Forms by Nonlinear Optical Stokes Ellipsometric Microscopy. *Anal. Chem.* **2016**, *88* (11), 5760–5768.
- (25) Toth, S. J.; Madden, J. T.; Taylor, L. S.; Marsac, P.; Simpson, G. J. Selective Imaging of Active Pharmaceutical Ingredients in Powdered Blends with Common Excipients Utilizing Two-Photon Excited Ultraviolet-Fluorescence and Ultraviolet-Second Order Nonlinear Optical Imaging of Chiral Crystals. *Anal. Chem.* **2012**, *84* (14), 5869–5875.
- (26) Toth, S. J.; Schmitt, P. D.; Snyder, G. R.; Trasi, N. S.; Sullivan, S. Z.; George, I. A.; Taylor, L. S.; Simpson, G. J. Ab Initio Prediction of the Diversity of Second Harmonic Generation from Pharmaceutically Relevant Materials. *Cryst. Growth Des.* **2015**, *15* (2), 581–586.
- (27) Wanapun, D.; Kestur, U. S.; Taylor, L. S.; Simpson, G. J. Single Particle Nonlinear Optical Imaging of Trace Crystallinity in an Organic Powder. *Anal. Chem.* **2011**, *83*, 4745–4751.
- (28) Chowdhury, A. U.; Ye, D. H.; Song, Z. T.; Zhang, S. J.; Hedderich, H. G.; Mallick, B.; Thirunahari, S.; Ramakrishnan, S.; Sengupta, A.; Gualtieri, E. J.; Bouman, C. A.; Simpson, G. J. Second Harmonic Generation Guided Raman Spectroscopy for Sensitive Detection of Polymorph Transitions. *Anal. Chem.* **2017**, *89* (11), 5958–5966.

- (29) Newman, J. A.; Schmitt, P. D.; Toth, S. J.; Deng, F. Y.; Zhang, S. J.; Simpson, G. J. Parts per Million Powder X-ray Diffraction. *Anal. Chem.* **2015**, 87 (21), 10950–10955.
- (30) Song, Z. T.; Sarkar, S.; Vogt, A. D.; Danzer, G. D.; Smith, C. J.; Gualtieri, E. J.; Simpson, G. J. Kinetic Modeling of Accelerated Stability Testing Enabled by Second Harmonic Generation Microscopy (vol 90, pg 4406, 2018). *Anal. Chem.* **2018**, *90* (21), 13130–13130.
- (31) Smith, C. J.; Dinh, J.; Schmitt, P. D.; Stroud, P. A.; Hinds, J.; Johnson, M. J.; Simpson, G. J. Calibration-Free Second Harmonic Generation (SHG) Image Analysis for Quantification of Trace Crystallinity Within Final Dosage Forms of Amorphous Solid Dispersions. *Appl. Spectrosc.* **2018**, 72 (11), 1594–1605.
- (32) Mistry, P.; Amponsah-Efah, K. K.; Suryanarayanan, R. Rapid Assessment of the Physical Stability of Amorphous Solid Dispersions. *Cryst. Growth Des.* **2017**, *17* (5), 2478–2485.
- (33) Kommanaboyina, B.; Rhodes, C. T. Trends in stability testing, with emphasis on stability during distribution and storage. *Drug Dev. Ind. Pharm.* **1999**, *25* (7), 857–868.
- (34) Moseson, D. E.; Mugheirbi, N. A.; Stewart, A. A.; Taylor, L. S. Nanometer-Scale Residual Crystals in a Hot Melt Extruded Amorphous Solid Dispersion: Characterization by Transmission Electron Microscopy. *Cryst. Growth Des.* **2018**, *18* (12), 7633–7640.